

Dynamics of Atmospheres and Oceans 33 (2001) 219–237



www.elsevier.com/locate/dynatmoce

Spin-up and spin-down in rotating fluid exhibiting inertial oscillations and frontogenesis

William Blumen*, Julie K. Lundquist

Program in Atmospheric and Oceanic Sciences, University of Colorado at Boulder, Campus Box 311, Boulder, CO 80309, USA

Received 2 February 2000; received in revised form 12 June 2000; accepted 31 July 2000

Abstract

Time-dependent, rotating flow in a finite depth of fluid is considered. Unbalanced initial conditions initiate flow in a shallow Ekman layer and in the inviscid interior, which is characterized by a state of zero potential vorticity. To determine the interior flow response to motion forced by the Ekman layer suction velocity, $w_{\rm B}$, an expansion of the flow to first-order in $E^{1/2}$, where E is the Ekman number, is carried out. Frontogenesis, which occurs in both the baroclinic and barotropic parts of the geostrophic flow, modulates the inertial oscillation that enters at zero order. A baroclinic front (infinite relative vorticity) can occur in a finite-time, equal to or less than one-half the period of an inertial oscillation, πf^{-1} These fast-time processes are described in detail by Blumen (2000).

Spin-up to the quasi-steady Ekman boundary layer solution also occurs during one-half the period of an inertial oscillation. Thereafter, $w_{\rm B}$ varies on a slow-time scale, $E^{-1/2}f^{-1}$. Yet, a barotropic front may form in a finite-time if the initial anticyclonic relative vorticity exceeds f, a condition that favors nonlinear steepening in opposition to boundary layer dissipation. This analysis contributes to a theoretical understanding of the interplay between spin-down and frontogenesis in rotating fluid. Some values of the Ekman number, typical of mid-latitude flows, are introduced to compare theoretical predictions to observed conditions. It is concluded that the Ekman layer corrections are most likely smaller in magnitude than the magnitude of errors in current atmospheric wind measurement systems, and therefore, not verifiable. Oceanic flows are also difficult to measure at the required accuracy, and other processes compete with Ekman layer dissipation to explain slow-time spin-down in the oceans. © 2001 Elsevier Science B.V. All rights reserved.

Keywords: Dissipation; Ekman layer; Frontogenesis; Inertial oscillation

* Corresponding author. Tel.: +1-303-492-7167; fax: +1-303-492-3524. *E-mail address:* blumen@paradox.colorado.edu (W. Blumen).

0377-0265/01/\$ – see front matter © 2001 Elsevier Science B.V. All rights reserved. PII: \$0377-0265(00)00062-2

1. Introduction

Inertial oscillations are fluid motions in level planes that are characterized by a period $\pi(\Omega\sin\phi)^{-1}$ where Ω is the Earth's rotation rate and ϕ denotes latitude. They are exact solutions of the equations of incompressible fluid motion when the pressure gradient and viscous forces are either small or balance each other. Viewed from a rotating frame, the velocity vector rotates in an anticyclonic or clockwise direction in the Northern Hemisphere, tracing out a circle (an inertial circle) during one period of the oscillation. Since these oscillations represent an exact solution of the equations of motion, they should be prominent in both atmospheric and oceanic data records in regions where both the pressure gradient and viscous forces are either negligible, or where the latter two forces are in balance.

Inertial oscillations have been observed below the surface mixed layer in the oceans and above the stable shallow nocturnal boundary layer of the atmosphere on many occasions. A particularly notable demonstration of the inertial oscillation in the ocean is displayed in Fig. 1. Warsh et al. (1971) show a power spectrum of motions at a depth of 25 m in the ocean near Barbados (13°N), where the inertial period is 52 h. Evidence for inertial oscillations in atmospheric data has also become established, e.g. Mori (1990) and Ostdiek and Blumen (1997). There have, however, been difficulties in extracting these oscillations from more data records for two principal reasons: firstly, the sampling rate of available instrumentation has not been adequate to resolve the oscillation (e.g. twice daily radiosonde soundings of the atmosphere) and, secondly, their contribution to power density spectral representations blends in with the diurnal spectral peak when atmospheric data are taken near $\phi = 30^{\circ}$ N. The observational facilities that provide sufficient temporal resolution are now largely in place:

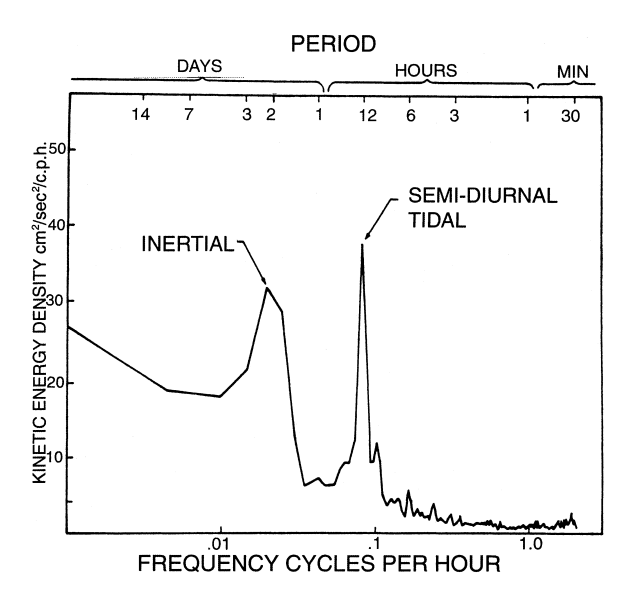


Fig. 1. Power spectrum of current speed at a depth of 25 m near Barbados (13°N) for the period 2 July to 13 August 1968. The inertial oscillation period is approximately 52 h (after Warsh et al. (1971)).

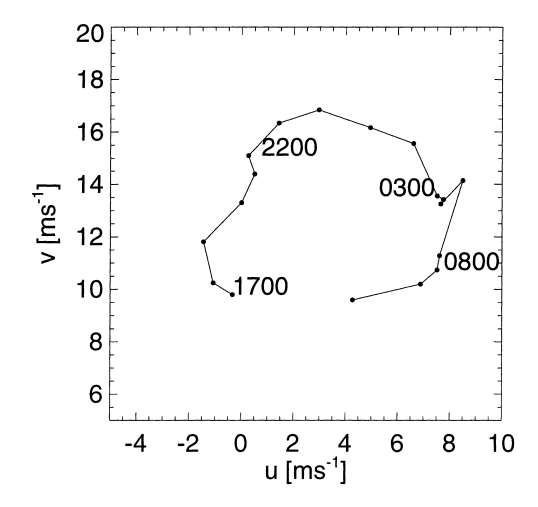


Fig. 2. Hodograph of an atmospheric inertial oscillation observed at 0.192 km with the Argonne Boundary-Layer Facility 915 MHz wind profiler at Whitewater, Kansas. The inertial period at this latitude is 19.5 h. The inertial oscillation takes place around steady-state wind values of $u_{ss} = 3.76 \,\mathrm{ms}^{-1}$, $v_{ss} = 12.61 \,\mathrm{ms}^{-1}$, with an amplitude of 4.19 ms⁻¹. The hours marked on the plot are in local daylight time (LDT): the inertial oscillation lasted from 17.00 h LDT on 11 October 1999 to 10.00 h LDT on 12 October 1999.

current meters used in ocean studies, and radar wind profilers for atmospheric investigations. Fig. 2 depicts an inertial oscillation observed with a UHF radar wind profiler.

Although observations of atmospheric inertial oscillations have increased recently (Singh et al., 1993; Banta et al., 1998), their sources are still being explored. The source of inertial oscillations in large bodies of water is largely accepted to be associated with winds that exert a stress at the air-ocean interface, and with the passage of storms and accompanying fronts that impart energy to the mixed layers of the oceans and large lakes (Kundu and Thomson, 1985; Tandon and Garrett, 1994). Other mechanisms are noted by Kunze and Sanford (1984), but will not be pursued here. A mechanism to excite inertial oscillations in the atmosphere was proposed by Blackadar (1957). It requires the development of a very stable layer close to the ground in association with radiative cooling in the late afternoon and early evening. The top of this layer, situated at a height $z \le 100 \,\mathrm{m}$, caps the layer where turbulent stresses are significant. Above this capping inversion lies the residual layer, a neutrally-stable convectively-mixed layer that is still present after the heat flux changes sign near sunset. The residual layer can accelerate if other constraining forces, like turbulent stresses, are absent. This method of initiating inertial oscillations in the residual layer up to 1-1.5 km has been reproduced in the model studies of Thorpe and Guymer (1977) and Singh et al. (1993), among others. These studies are, however, not definitive because their models are built upon the Blackadar mechanism: inertial oscillations are assumed to occur in the residual layer. In contrast, Ostdiek and Blumen (1997) have documented the occurrence of inertial oscillations during the passage of a weak cold front in the Southern Great Plains, when the atmosphere was neutrally stratified from the ground up to a height of several hundred meters. Inertial oscillations were detected by means of boundary-layer profilers and surface observations, and were even evident at the 10 m level at a number of locations. Low-level mixing by surface winds, associated with the frontal progression, appears to have prevented the development of the nocturnal stable layer during this event. Frontal initiation of inertial oscillations is suggested.

The possibility of inertial oscillations that co-exist with frontal passages raises some interesting dynamical consequences. Balanced models, such as the semigeostrophic model, are often used in mesoscale atmospheric and oceanic studies because they appear to capture relatively realistic atmospheric frontogenesis without having to expend additional computational resources on a primitive equation model. A principal question that arises concerns the relative contribution of inertial oscillations to both the inception and decay of a front, called frontogenesis and frontolysis.

Blumen (1997) showed that inertial oscillations could be modulated by semigeostrophic frontogenesis, but the reverse process was not attainable by the method of analysis employed. A zero-potential-vorticity (ZPV) model was employed later by Blumen (2000) to establish that there is a significant interaction between inertial oscillations and frontogenesis. In fact, the relevance of this model of frontogenesis was demonstrated earlier by Blumen et al. (1996) in application to a frontogenesis event in the Great Plains. In that event, the frontal width decreased from a few tens of kilometers to a few hundred meters within a period of about 3 h. Dissipation of turbulent kinetic energy within the frontal zone prevents the development of a temperature or wind discontinuity, and ultimately frontolysis takes over. Sanders (1999) recently provided an analysis of frontogenesis in the Southwestern United States that exhibited similar spatial and temporal characteristics, but he did not carry out any model study to evaluate the impact of inertial oscillations on frontogenesis. The essence of this nonlinear interaction will be reviewed below.

The purpose of the present study is to extend the work presented in Blumen (2000) to include an Ekman boundary layer. The basic equations and a brief summary of the mathematical approach is provided in Section 2. Next the linear, time-dependent Ekman boundary layer solution is introduced, and the Ekman suction velocity is determined in Section 3 and Appendix A. The analysis of frontogenesis when an Ekman suction velocity provides a lower boundary condition is taken up in Section 4. The analysis follows very closely the approach provided by Greenspan (1990), in the reissue of his 1968 edition. As might be anticipated, the development is one of spin-up of the boundary layer from a state of rest until a quasi-steady Ekman boundary layer is achieved, and the interior motion reveals a secondary circulation in response to the presence of the Ekman layer. Then the barotropic part of the basic state geostrophic flow spins down, leaving the baroclinic part of the geostrophic flow and modulated inertial oscillations intact. A summary of the principal conclusions, and some remarks on geophysical relevance, appear in Section 5.

The emphasis in this study is placed on frontogenesis, and particularly on the role of the Ekman boundary layer in its development. This aspect of the spin-up and spin-down problem has apparently not been emphasized in previous studies. The intention is to examine this problem in geophysical settings, albeit very ideal ones, in order to establish the various time scales that are appropriate to oceanic and atmospheric situations, and to provide insights into frontogenesis when non-steady inertial oscillations and the boundary layer play a role.

2. The inviscid model

The inviscid model, which represents the basic state dynamics, has been presented by Blumen (2000), hereafter BL. The Ekman layer enters at first-order in an expansion in terms of $E^{1/2}$, where E is the Ekman number. The Ekman layer is placed below the inviscid interior flow for atmospheric applications; it may be placed above the inviscid interior flow for oceanic applications. This alteration does not change any of the physical interpretations that are presented. The plan is to introduce the model equations, apply the absolute momentum coordinate transformation, which eliminates some nonlinear terms, solve a linear problem in coordinate space, and then return to physical space for clearer interpretation of the solution. Along-front variability is observed, in both oceanic and atmospheric fronts, to be negligibly small ($\partial/\partial y \approx 0$) in comparison with rapid changes in both the temperature and wind fields that occur across the frontal zone. As a consequence, the basic equations are those of two-dimensional, inviscid and rotating flow with the Boussinesq approximation applied. These equations, representing the horizontal equations of motion, hydrostatic balance, continuity and conservation of potential temperature (replaced by temperature under the Boussinesq approximation) are expressed as

$$\frac{\partial u}{\partial t} + u \frac{\partial u}{\partial x} + w \frac{\partial u}{\partial z} - fv = -\frac{\partial \pi}{\partial x},\tag{1}$$

$$\frac{\partial v}{\partial t} + u \frac{\partial v}{\partial x} + w \frac{\partial v}{\partial z} - fu = 0, \tag{2}$$

$$0 = -\frac{\partial \pi}{\partial z} + g \frac{\theta}{\theta(0)},\tag{3}$$

$$\frac{\partial u}{\partial x} + \frac{\partial w}{\partial z} = 0,\tag{4}$$

$$\frac{\partial}{\partial t} \frac{\theta}{\theta(0)} + u \frac{\partial}{\partial x} \frac{\theta}{\theta(0)} + w \frac{\partial}{\partial z} \frac{\theta}{\theta(0)} = 0, \tag{5}$$

where (u, v, w) are velocity components in the (x, y, z) directions, $\partial/\partial y = 0$, $\pi = p/\rho(0)$ (p is the pressure and $\rho(0)$ the reference density), $\theta/\theta(0)$ the ratio of the temperature to a reference temperature, g the acceleration of gravity, and the Coriolis parameter f is constant. The reference values $\rho(0)$ and $\theta(0)$ refer to values at the level between the inviscid layer and the Ekman layer. Absolute momentum coordinates

$$X = x + v/f, \qquad Z = z, \qquad T = t \tag{6}$$

are introduced into Eqs. (1)–(5). The motions are constrained by the assumption that the potential vorticity is set equal to zero for purposes of mathematical simplification. This condition is equivalent to $\partial(\theta/\theta(0))/\partial Z = 0$. A desirable property of this system, which is evident from (2), is the conservation of X following the motion. The relative simplicity of the transformed set of equations, and ease of interpretation, is a by-product of this latter conservation principle. The transformation to absolute momentum coordinates yields

$$\frac{\partial u_{\mathbf{a}}}{\partial T} + w \frac{\partial u_{\mathbf{a}}}{\partial Z} - f v_{\mathbf{a}} = 0, \tag{7}$$

$$\frac{\partial v}{\partial T} + w \frac{\partial v}{\partial Z} + f u_{\rm a} = 0, \tag{8}$$

$$\frac{\partial}{\partial X} \left(u_{\mathbf{a}} + f^{-1} w \frac{\partial v}{\partial Z} \right) + \frac{\partial}{\partial Z} \left(1 - f^{-1} \frac{\partial v}{\partial X} \right) w = 0, \tag{9}$$

$$\frac{\partial}{\partial T} \frac{\theta}{\theta(0)} = 0,\tag{10}$$

where u_a denotes the ageostrophic component, and $v = v_g + v_a$ is composed of both a geostrophic and an ageostrophic component of motion. The complete development appears in BL, particularly in Appendix A. Geostrophic and hydrostatic balance, not displayed above, will be developed further. Geostrophic balance is represented by

$$v_{\rm g} = f^{-1} \frac{\partial \pi}{\partial x} \tag{11}$$

and hydrostatic balance by (3). Transformation of Eqs. (11) and (3) by means of (6) (or see Hoskins (1975)) yields

$$v_{\rm g} = f^{-1} \frac{\partial \Pi}{\partial X}, \qquad 0 = \frac{-\partial \Pi}{\partial Z} + \frac{g\theta}{\theta(0)},$$
 (12)

where

$$\Pi = \pi + \frac{v_{\rm g}^2}{2} \tag{13}$$

These results are in agreement with the transformed variables displayed by Hoskins (1975), who used the geostrophic coordinate transformation, (6), with v replaced by v_g . Agreement with geostrophic coordinates in the in the representation of Eqs. (12) and (13) occurs because the horizontal pressure field is completely represented by geostrophic balance. The ageostrophic flow and the accelerations in Eqs. (7) and (8) are unaffected by both the pressure gradient and viscous forces. Inertial oscillations are described by this system of equations, but not internal gravity waves, as a consequence of the ZPV assumption. It follows from ZPV and (10) that $\theta/\theta(0)$ is only a function of X. As a consequence, the two expressions in (12) may be combined to yield the baroclinic part of the geostrophic velocity, provided by

$$\hat{v} = -\frac{g}{f} \frac{\partial}{\partial X} \frac{\theta}{\theta(0)} \left(\frac{h}{2} - Z \right),\tag{14}$$

where the flow is confined to a channel, $0 \le Z \le h$. The barotropic part of v_g will be represented as

$$\bar{v} = \frac{1}{f} \frac{\partial}{\partial X} \bar{\Pi}. \tag{15}$$

Both $\theta/\theta(0)$ and the barotropic pressure field $\bar{\Pi}$ need to be specified. Periodic boundary conditions are used, as in BL, to insure that there is no net horizontal mass flux, although (14) already satisfies this condition because its vertical average vanishes. The initial conditions

appropriate to this model are

$$u_{\rm a} = w = v_{\rm g} + v_{\rm a} = 0, \quad T = 0,$$
 (16)

where $v_g = \hat{v} + \bar{v}$. The zero-order baroclinic part of the flow may be determined from Eqs. (7)–(9) with w = 0 at the level boundaries (0, h). This solution will only be considered, however, at z = Z = 0. Approximate interior solutions have been presented in BL, but they need not be considered in the present analysis. The exact solutions that satisfy Eqs. (7), (8) and (16) at Z = 0 are

$$v = \hat{v}(1 - \cos fT)$$

$$u_{a} = -\hat{v}\sin fT$$

$$w = 0$$

$$, \qquad (17)$$

where \hat{v} is given by (14).

The most significant aspect of this solution, for present purposes, is the fact that (17) represents the solution in physical space with T replaced by t and $\hat{v} = \hat{v}(x,t)$ at z = 0. Thus, the zero-order solution is represented by a modulated inertial oscillation superposed on a baroclinic geostrophic flow, which evolves on a fast time scale. The barotropic part of the geostrophic flow evolves on a slow time scale, much longer than one inertial period. This development is deferred until Section 4.3. It will also be shown in Section 4 that barotropic frontogenesis takes place in the v_g field, but that there are differences between baroclinic and barotropic frontogenesis.

3. The boundary layer model

A multitude of time-dependent Ekman boundary layer solutions appear in the literature. The solution presented by Pandolfo and Brown (1967) represents the appropriate model solution for this study. This solution (19) satisfies the initial conditions (16) and approaches the steady-state Ekman boundary layer solution:

$$u + iv = iv_g \left\{ 1 - \exp\left[-(1+i)\frac{z}{\delta_{\rm E}} \right] \right\}$$
 (18)

when z is finite and $t \to \infty$. This limiting solution (18) is actually approached within less than one inertial period, and the barotropic part of v_g varies on a slow time scale, to be introduced below. The solution is represented by

$$u + iv = \frac{1}{2}iv_{g} \left\{ \exp\left[(1+i)\frac{z}{\delta_{E}} \right] \operatorname{erfc}\left[\frac{z}{2\delta_{E}} \left(\frac{ft}{2} \right)^{-1/2} + (1+i) \left(\frac{ft}{2} \right)^{1/2} \right] \right.$$

$$\left. + \exp\left[-(1+i)\frac{z}{\delta_{E}} \right] \operatorname{erfc}\left[\frac{z}{2\delta_{E}} \left(\frac{ft}{2} \right)^{-1/2} - (1+i) \left(\frac{ft}{2} \right)^{1/2} \right] \right\}$$

$$\left. + iv_{g} \left[1 - \operatorname{erf}\left(\frac{z}{2\delta_{E}} \left(\frac{ft}{2} \right)^{-1/2} \right) \exp(-ift) \right], \tag{19}$$

where $\operatorname{erfc}(y) = 1 - \operatorname{erf}(y)$ is the complementary error function and

$$\operatorname{erf}(y) = 2\pi^{-1/2} \int_0^y e^{-t^2} dt$$
 (20)

is the error function (Gautschi, 1964). The parameter δ_E is the Ekman layer thickness, defined as $\delta_E = (2\kappa f^{-1})^{1/2}$, where κ is a constant eddy viscosity coefficient. Characteristic values for the atmosphere and the oceans will be introduced in Section 5. It is only necessary at this time to require that $E^{1/2} = \delta_E h^{-1} \ll 1$ in this channel model. At infinite height, the top of the boundary layer, the solution is characterized by

$$u + iv \rightarrow iv_g(1 - \exp(-ift)), \quad z \rightarrow \infty$$
 (21)

which is in agreement with (17) when T is replaced by t.

Integration of the continuity Eq. (4) through the depth of the boundary layer provides the Ekman suction velocity

$$w_{\rm B} \approx \frac{\delta_{\rm E}}{2} \frac{\partial v_{\rm g}}{\partial x} \left[\operatorname{erf} \left(\frac{ft}{2} \right)^{1/2} + \frac{\exp(-ft/2)}{2\pi (ft/2)^{1/2}} (1 - \cos ft - \sin ft) \right]. \tag{22}$$

The development appears in Appendix A, and w_B is shown as a function of time in Fig. 3. The time scale for spin-up to the asymptotic value

$$w_{\rm B} = \frac{\delta_{\rm E}}{2} \frac{\partial v_{\rm g}}{\partial x},\tag{23}$$

is less than the period of one inertial oscillation, in approximate agreement with the results presented by Greenspan (1990, Fig. 2.3). To summarize, the time-dependent solution (18) asymptotically matches the interior solution at the base of the upper layer, z = 0. Exchange between the interior fluid and the boundary layer will take place at z = 0, where (22) will serve as a lower boundary condition for the boundary layer correction to the zero-order inviscid solution (17).

4. Spin-up, spin-down and frontogenesis

Greenspan (1990) has provided a clear physical discussion and mathematical formulation of the spin-up and spin-down process. The specific model is one that is realizable in a laboratory setting, although his presentation would be applicable to geophysical environments as well (see, in particular, Chapter 2 and Section 3.7).

The present approach, as in Greenspan's development, is to define a zero-order basic-state, modify the basic-state, and display the secondary interior circulation in response to the boundary layer transport at the base of the interior fluid layer. As he notes, "the procedure continues until the mutual interactions of the interior and boundary layer flows are determined to the desired accuracy."

Frontogenesis and the forced secondary circulation are clearly evident when the solution is terminated at order $E^{1/2}$, where E is the Ekman number. As in Greenspan's development, each contribution to the solution will be examined separately. The distinction is made

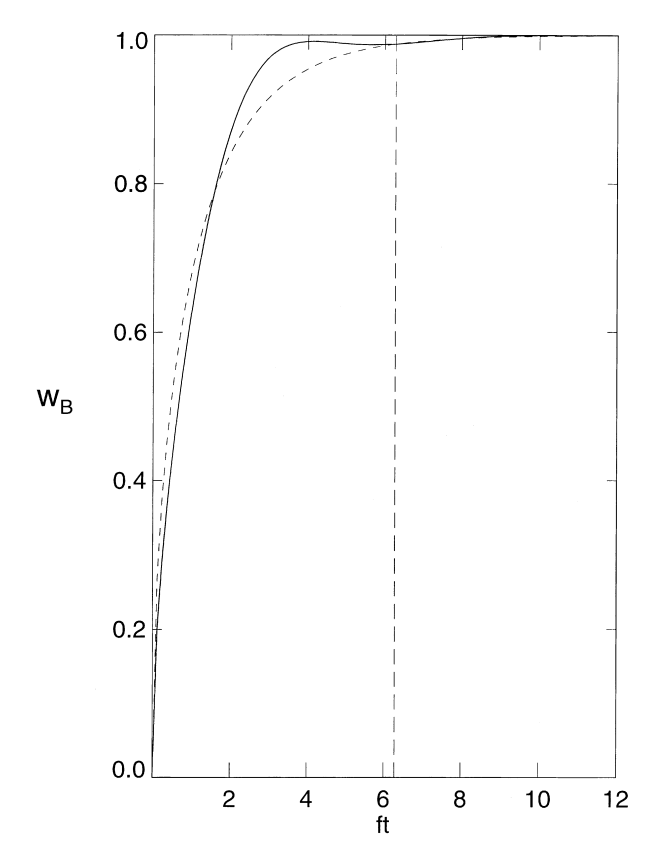


Fig. 3. Ekman suction velocity $w_{\rm B}$ (solid line) as a function of nondimensional time ft, provided by (22). The velocity has been normalized by its asymptotic value $w_{\rm B} = (\delta_{\rm E}/2) \partial v_{\rm g}/\partial x$. The short-dashed line is the representation of $w_{\rm B}$ by the first term in (22), and the long-dashed vertical line is $ft = 2\pi$.

between motions that occur on a fast-time scale $t \sim f^{-1}$ and those that evolve on a slow-time scale $t \sim E^{-1/2}f^{-1}$, where $E^{1/2} \ll 1$.

4.1. Fast-time: zero-order

The zero-order, fast-time solution is presented in (17). It is composed of a geostrophic flow, the baroclinic part, and superposed inertial oscillations that are both characterized by order f^{-1} variation. The barotropic part of the geostrophic flow varies on a slow-time scale, and so is effectively constant on this fast time-scale, and may be omitted. The easiest way to display the fast-time variation of the geostrophic flow is to replace T by t in (17) and substitute this solution into either Eq. (1) or (2). The result, developed in BL (Section 4), is a nonlinear advection equation for the baroclinic part of the geostrophic flow (14), given by

$$\left(\frac{\partial}{\partial \tau} - \hat{v}\frac{\partial}{\partial x}\right)\hat{v} = 0,\tag{24}$$

where $\tau = f^{-1}(1 - \cos ft)$. The time-scale for frontogenesis may be determined from (24), as in Lighthill (1978, Section 2.9). Differentiation of (24) with respect to x and rearrangement produces

$$\left(\frac{\partial}{\partial \tau} - \hat{v}\frac{\partial}{\partial x}\right) \left(\frac{\partial \hat{v}}{\partial x}\right)^{-1} = \frac{\mathrm{d}}{\mathrm{d}\tau} \left(\frac{\partial \hat{v}}{\partial x}\right)^{-1} = -1. \tag{25}$$

Steepening of \hat{v} occurs by nonlinear self-advection, and $\partial \hat{v}/\partial x$ may become infinite at $\tau = \tau_c$. Integration of (25) from $t = \tau = 0$ to τ yields

$$1 - \cos ft_{\rm c} = \frac{1}{f^{-1} \partial \hat{v} / \partial x|_{0}},\tag{26}$$

where the right hand side of (26) is evaluated at $t = \tau = 0$. The maximum value of the left hand side of (26) is 2, so that a front $(\partial \hat{v}/\partial x) = \infty$ can only form if the initial relative vorticity satisfies $f^{-1}\partial \hat{v}/\partial x|_0 \geq 0.5$; otherwise a front will not form. Frontolysis occurs in the interval $\pi < ft \leq 2\pi$. Frontal development is displayed in BL. The present formulation can only proceed if a front does not form, otherwise the solution cannot be extended past $t = t_c$. For present purposes, the fast-time zero-order solution will be represented as a baroclinic geostrophic flow that alternately undergoes frontogenesis and frontolysis on a fast-time scale, and a modulated inertial oscillation. The possibility of symmetric instability of this flow has been raised by Tandon and Garrett (1994) but, as shown in BL, this possibility is excluded because the potential vorticity cannot become negative.

4.2. Fast-time: first order

An appropriate ordering of the solutions is facilitated by introduction of nondimensional scales. The following apply:

$$x = \lambda x', \quad z = hz', \quad t = f^{-1}t', \quad (u, v) = (g^*h)^{1/2}(u', v'),$$

 $w = fhw', \quad \theta/\theta(0) = \Theta\theta'.$

The primed variables are nondimensional, Θ is a characteristic amplitude of the initial temperature field:

$$g^* = g\Theta, \qquad \lambda = (g^*h)^{1/2} f^{-1}$$

and δ_E is defined below (20). The prime notation will now be dropped. The Ekman suction velocity (22) may be written as

$$w_{\rm B} = E^{1/2} \frac{1}{2} \frac{\partial v_{\rm g}}{\partial x} [1 - F(t)],$$
 (27)

where

$$F(t) = \operatorname{erfc}\left(\frac{t}{2}\right)^{1/2} - \frac{\exp(-t/2)}{2\pi(t/2)^{1/2}}(1 - \cos t - \sin t). \tag{28}$$

Spin-up to the asymptotic value, $w_{\rm B} = 1/2E^{1/2}\partial v_{\rm g}/\partial x$ is a fast-time process as noted in Section 3, with $F(t) \to 0$ over a characteristic interval $t \sim \pi f^{-1}$.

4.3. Slow-time: first-order

The slow-time evolution of v_g remains to be determined. The geostrophic velocity is a zero-order variable, but it is necessary to proceed to the first-order equations to determine the barotropic slow-time evolution. A two-time scale expansion is an appropriate method to pursue, since E represents the ratio of the rotation period to a characteristic diffusion time. Since the fast-time processes have already been isolated, it is preferable to follow Greenspan's (1990, Section 3.7) approach, and simply rescale the time in order to isolate the slow-time variation. That is, t is now scaled as $t = E^{-1/2} f^{-1} t'$.

The analysis is simplified by first exploiting the simplification provided by the use of absolute momentum coordinates. The same nondimensionalization is applied to the transformed variables, and the solution expanded as

$$u_{a} = E^{1/2}u_{a1} + \cdots
 v = \bar{v} + E^{1/2}v_{a1} + \cdots
 w = E^{1/2}w_{1} + \cdots$$
(29)

The zero-order flow with this new scaling is the barotropic part of the geostrophic flow

$$\bar{v} = \frac{\partial \bar{\Pi}}{\partial X},\tag{30}$$

where \bar{v} is now the nondimensional representation of (15). Although the baroclinic part of the geostrophic flow is independent of time in transformed space according to Eqs. (14) and (10), the fast-time variation of the baro clinic geostrophic flow is revealed in the transformation back to physical space (24). The baroclinic part of the geostrophic flow and the inertial oscillations do not appear at zero-order with the deployment of the slow-time scale. Eqs. (8) and (9) are order $E^{1/2}$ representations, which may be expressed as

$$\frac{\partial \bar{v}}{\partial T'} + u_{a1} = 0, (31)$$

$$\frac{\partial}{\partial X}u_{a1} + \frac{\partial}{\partial Z}\left(1 - \frac{\partial\bar{v}}{\partial X}\right)w_1 = 0,\tag{32}$$

where the prime notation is retained here as a reminder that T' is a slow-time variable. On this time-scale, the Ekman suction velocity at z = 0, represented by (27), does not retain the fast-time representation F(t), given by (28). It may be expressed in transformed variables as

$$\left(1 - \frac{\partial \bar{v}}{\partial X}\right) w_{\rm B} = \frac{1}{2} \frac{\partial \bar{v}}{\partial X}, \quad Z = 0$$
(33)

where $\partial/\partial x = (1 - \partial v/\partial X)^{-1}\partial/\partial X$ and v is evaluated by \bar{v} to leading order. The slow-time behavior of \bar{v} is determined from (31) after u_{a1} is determined. As in BL, the relative simplicity of Eqs. (31) and (32) may be exploited further by introduction of two new variables

$$u^* = u_{a1} w^* = \left(1 - \frac{\partial \bar{v}}{\partial X}\right) w_1$$
 (34)

which were first introduced by Hoskins and Draghici (1977). Then Eqs. (31) and (32) reduce to

$$\frac{\partial \bar{v}}{\partial T'} + u^* = 0, (35)$$

$$\frac{\partial u^*}{\partial X} + \frac{\partial w^*}{\partial Z} = 0. {36}$$

Integration of (36), noting that $w = w^* = 0$ at the level boundary Z = 1, yields

$$\frac{\partial}{\partial X} \int_0^1 u^* \, \mathrm{d}Z = w^*(X, 0, T') = \frac{1}{2} \frac{\partial \bar{v}}{\partial X},\tag{37}$$

where w^* is expressed by the right hand side of (33), the slow-time Ekman representation in transformed coordinates. It is only the barotropic part of the geostrophic flow \bar{v} in (31) that evolves on the slow-time, so that u^* must be barotropic and, from (37)

$$u^* = \frac{1}{2}\bar{v}(X, T'). \tag{38}$$

Introduction of Eq. (38) into Eq. (35), followed by one integration, yields

$$\bar{v} = \bar{v}(x_0) e^{-T'/2},$$
 (39)

where $X = x_0$ at T' = 0. The barotropic part of the geostrophic flow spins down at a rate $E^{1/2} f/2$. This spin-down rate is a well-known result, e.g. Greenspan (1990). The fact that frontogenesis occurs simultaneously has apparently not been recognized.

The secondary circulation may also be determined. The vertical velocity is determined from Eqs. (36) and (38), and expressed as

$$w^* = \frac{1}{2} \frac{\partial \bar{v}}{\partial X} (1 - Z) \tag{40}$$

Both u_{a1} and w_1 may be determined from (34), since u^*, w^* , and \bar{v} have been determined. Streamlines of the secondary circulation, represented by Eqs. (38) and (40) in transformed space, will be presented in Section 5.

4.4. Spin-down and frontogenesis

The final steps in this analysis are to return to physical space and to interpret the barotropic slow-time response. One way is to evaluate (2) using the physical space representation of u_{a1} and w_1 , obtained from Eqs. (34) and (40). The more direct route is to note that (39) provides

$$\frac{\partial \bar{v}}{\partial T'} = -\frac{1}{2}\bar{v}.\tag{41}$$

The reverse transformation is found from

$$\frac{\partial \bar{v}}{\partial T'} = \frac{\partial \bar{v}}{\partial t'} - \left(\frac{\partial \bar{v}}{\partial x}\right) \frac{\partial \bar{v}}{\partial T'}$$

where x = X - v from the nondimensional form of (6). Rearrangement yields

$$\frac{\partial \bar{v}}{\partial T'} = \left(1 + \frac{\partial \bar{v}}{\partial x}\right)^{-1} \frac{\partial \bar{v}}{\partial t'}.\tag{42}$$

Now Eqs. (41) and (42) may be combined to yield an equation for the barotropic geostrophic velocity in physical space. The dimensional representation of this equation is

$$\frac{\partial \bar{v}}{\partial \bar{\tau}} + \frac{1}{2} \bar{v} \frac{\partial \bar{v}}{\partial x} + \frac{f}{2} \bar{v} = 0, \tag{43}$$

where $\bar{\tau} = E^{1/2}t$ will be used in the developments that follow. Eq. (43) expresses the slow-time evolution of \bar{v} : it describes nonlinear steepening (frontogenesis), as in (24), that is opposed by linear damping (spin-down). This equation has been analyzed by Whitham (1974, Section 2.12). Pedlosky (1987, Section 4.3) has shown that the rate at which energy is supplied, \dot{W} , to maintain the asymptotic-state of the Ekman layer against frictional dissipation is, in the present units

$$\dot{W} = f\rho(0) \left\langle \frac{\bar{v}^2}{2} \right\rangle,\tag{44}$$

where $\langle \rangle$ denotes a volume average. He notes that, since the pressure is the same in the interior as in the Ekman layer, the rate of energy loss in the interior is (44) with the sign reversed. Multiplication of (43) by $\rho(0)$ and integration over x for this barotropic flow provides

$$\frac{\partial}{\partial \bar{\tau}} \rho(0) \left\langle \frac{\bar{v}^2}{2} \right\rangle = -f \rho(0) \left\langle \frac{\bar{v}^2}{2} \right\rangle,\tag{45}$$

which is the energy loss in the interior.

According to Whitham's (1974, Section 2.12) analysis, (43) may be expressed as

$$\frac{\mathrm{d}}{\mathrm{d}\bar{v}}\bar{v} + \frac{f}{2}\bar{v} = 0,\tag{46}$$

where $dx/d\bar{\tau} = \bar{v}/2$ (further development is by the method of characteristics). The equivalent representation of (46) is the conservation of absolute linear momentum

$$\frac{\mathrm{d}}{\mathrm{d}\bar{x}}(\bar{v} + fx) = 0. \tag{47}$$

Fluid parcels move outward and away from the point of fluid injection into the interior, and the cyclonic circulation decreases to satisfy (47). Downward injection of interior fluid into the Ekman layer requires a decrease in the anticyclonic circulation as the rotation axis is approached. Finally, the interplay between nonlinear advection and dissipation may be displayed by rewriting (47) as

$$\bar{v}(x,\bar{\tau}) + fx = \bar{v}(x_0) + fx_0,$$
 (48)

where x_0 designates the x-coordinate representation at $\bar{\tau} = 0$. This expression (48) represents a desired relationship between the coordinate positions x and x_0 after $\bar{v}(x, \bar{\tau})$ is

expressed in terms of $\bar{v}(x_0)$. This latter relationship is provided in nondimensional terms by (39). Transformation to dimensional units and introduction into (48) provides

$$x = x_0 + f^{-1}\bar{v}(x_0)(1 - e^{-f\bar{\tau}/2}),\tag{49}$$

where $\bar{\tau}$ is defined below (43). Andrews and Hoskins (1978) have shown that a discontinuity will occur at $\bar{\tau} = \bar{\tau}_c(\partial \bar{v}/\partial x = \infty)$ when $\partial x/\partial x_0 = 0$. This latter condition determines the time $\bar{\tau}_c$ when x ceases to be a single-valued function of x_0 . In the present case, the discontinuity or front will occur at $\bar{\tau} = \bar{\tau}_c$ given by

$$1 - \exp\left[\frac{-f\bar{\tau}_{c}}{2}\right] = \frac{1}{f^{-1}|\partial\bar{v}/\partial x_{0}|},\tag{50}$$

where frontal formation is restricted to anticyclonic flow, $\partial \bar{v}/\partial x_0 < 0$. Further, a large initial anticyclonic vorticity is required to produce a front, $|\partial \bar{v}/\partial x_0| > f$, because frontogenesis is occurring as the fluid spins down.

It is interesting to contrast frontogenesis that occurs on different time scales. It is demonstrated in BL that the fast-time inertial oscillation collaborates with nonlinear self-advection to accelerate frontogenesis during the first half-cycle of the oscillation, $0 < ft \le \pi$. The initial cyclonic vorticity need only exceed f/2 for a front to form, as established by (26). In contrast, frontogenesis on the slow-time scale has to overcome the damping effect of Ekman dissipation to produce a front. Relatively large initial anticyclonic vorticities are required, $|\partial \bar{v}/\partial x_0| > f$, to permit this to occur as established by (49). An evaluation will be provided in Section 5. The reason that frontogenesis is associated with geostrophic vorticities of opposite sign is related to the divergence field. Convergence, associated with positive relative vorticity, produces a front at the pressure minimum, in which low density fluid overlies high density fluid. Alternatively, interior flow forced by the Ekman suction velocity produces convergence at the pressure maximum, where the relative vorticity is negative and where fluid is removed from the interior to supply divergent motion in the Ekman layer. The latter type of frontogenesis is a barotropic process.

5. Summary and remarks

The analysis procedure outlined at the beginning of Section 4 has been carried out, restricting attention to order $E^{1/2}$ effects produced in the interior flow by the presence of the Ekman boundary layer. Ekman layer suction provides the order $E^{1/2} \ll 1$ corrections to (17) and, as a consequence, the boundary layer solution (18) only matches the interior flow at zero-order as shown by (21). The iterative process noted by Greenspan (1990), whereby the mutual interaction between the boundary layer and interior flows are matched to a higher degree of accuracy, is not carried out. The principal conclusions of this study, frontogenesis during spin-down, are stated at the end of Section 4, and details of the fast-time, baroclinic response are provided in BL. The complete solution, to order $E^{1/2}$, is represented in physical space by

$$v = v_{\rm g}(1 - \cos ft),\tag{51}$$

$$u_{\rm a} = -v_{\rm g}\sin ft + \frac{1}{2}\frac{\delta_{\rm E}}{h}\bar{v},\tag{52}$$

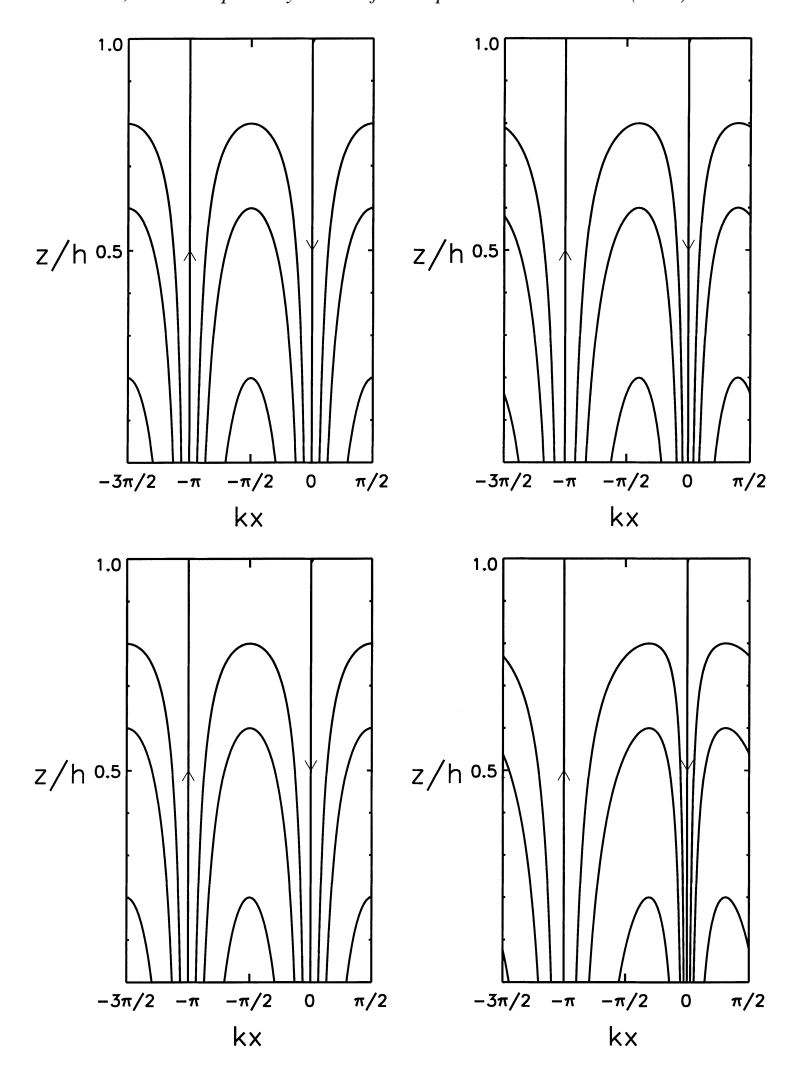


Fig. 4. Streamlines of the first-order ageostrophic flow in physical space $(kx, h^{-1}z)$, where k is the x-wavenumber of the barotropic geostrophic flow, and h is the channel depth. The top and bottom panels are, respectively, $f^{-1}|\partial \bar{v}/\partial x_0|=(0.5,0.95)$. The left- and right-hand side panels are, respectively, times ft=0 and ft=20. Downwelling occurs in the vicinity of kx=0.

$$w_1 = \frac{1}{2} \frac{\delta_{\rm E}}{h} \frac{\partial \bar{v}}{\partial x} (h - z) \tag{53}$$

where the order $\delta_{\rm E}/h$ terms are determined from Eqs. (34), (38) and (40) and transformed to physical space. The baroclinic part of the geostrophic velocity in Eqs. (51) and (52) is determined by (24), and the barotropic part by (43). The streamlines for the ageostrophic flow (u_{a1}, w_1) are shown in Fig. 4 for the case of a cyclic representation, $\bar{v} = -V \sin kx_0$ where V denotes the amplitude and k is the x-wavenumber. According to the present development,

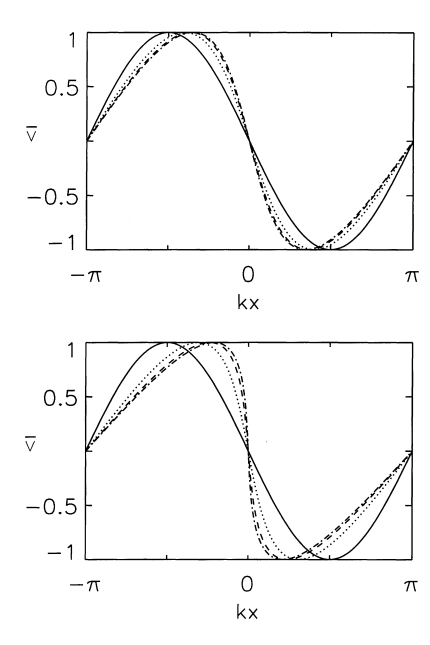


Fig. 5. Barotropic geostrophic flow \bar{v} , normalized by $\exp(-fE^{1/2}t/2)$ vs. the nondimensional coordinate kx. The top and bottom panels are, respectively, $f^{-1}|\partial \bar{v}/\partial x_0|=(0.5,0.95)$. The times are: $fE^{1/2}t=0$ (solid), 2 (dotted), 4 (dashed), 6 (dashed-dot).

the inertial oscillation, in Eqs. (51) and (52), is set up from the onset by the specification of unbalanced initial conditions. The oscillation is modulated by both a fast-time baroclinic flow and a slow-time barotropic flow. The frontogenetic properties of the barotropic flow are displayed in Fig. 5. The increase in the gradient of \bar{v} is a consequence of convergent cross-isobar ageostrophic flow, displayed in Fig. 4. The use of a linear Ekman boundary layer solution becomes less valid as this nonlinear interior process proceeds. The tendency for frontogenesis in anticyclonic flow would, however, not change when a nonlinear correction to the Ekman suction velocity is incorporated. Hart (2000) has shown that the magnitude of the suction velocity increases in anticyclonic flow, but that the direction of the forced secondary flow is unaltered.

Although a finite frontal-width is approached as $\bar{\tau}=E^{1/2}t$ increases, the amplitude of \bar{v} is essentially zero when $f\bar{\tau}/2=3$. A typical value of $E^{1/2}$, which characterizes midlatitude atmospheric motions, is $E^{1/2}\approx 10^{-1}$, with the Ekman depth $\delta_{\rm E}\approx 300-450\,{\rm m}$ (Holton, 1992, Chapter 5). A typical oceanic value is $E^{1/2}\approx 10^{-2}\,{\rm or}$ less, with $\delta_{\rm E}\leq 10\,{\rm m}$ (Cushman-Roisin, 1994). According to (39), the e-folding times, $T_{\rm E}=2E^{-1/2}f^{-1}$, are, respectively, 2–3 days for the atmosphere, and 3 weeks or longer for the oceans. Little evidence for spin-down should be apparent during the period from dusk to dawn in the atmosphere. As noted earlier, spin-down opposes frontogenesis. According to (50), relatively large initial values of anticyclonic vorticity are required to produce frontal formation in a finite time; the occurrence of frontal formation at the e-folding time for example, requires $|\partial \bar{v}/\partial x_0|f^{-1}\approx 1.6$. Anticyclonic relative vorticities of this magnitude would not normally be observed in mesoscale atmospheric flow, because negative absolute vorticity is expected

to be an unstable state, e.g. Holton (1992, Section 7.5). The secondary circulation, on the other hand, spins up according to (22) and Fig. 3 during the first half-cycle of the inertial period. Values of u_{a1} and w_{B} would have typical atmospheric values

$$\begin{split} u_{\rm a1} &\approx \frac{1}{2} \frac{\delta_{\rm E}}{h} v_{\rm g} \approx \frac{1}{20} \times 10 \approx 0.5 \, \rm ms^{-1}, \\ w_{\rm B} &\approx \frac{1}{2} \delta_{\rm E} \frac{\partial v_{\rm g}}{\partial x} \approx \frac{1}{2} \times 400 \times \frac{1}{2} \times 10^{-4} \approx 10^{-2} \, \rm ms^{-1}. \end{split}$$

The secondary circulation would be very difficult to measure with radar wind profilers, for example, because it would be swamped by the wind measurement errors. Although the velocities would increase with a decrease in f, the spin-up time would also increase, and the circulation would become obscured by convective activity after sunrise. Spin-up and spin-down are important fluid dynamical constructs upon which to gain insights about the effects of the planetary boundary layer on interior fluid motions. It is, regrettably, difficult to evaluate either the short- or long-term effects on atmospheric motions, at least through Ekman layer dynamics. The oceans may offer more suitable conditions for boundary layer influences to be evaluated. Inertial oscillations may persist for several days, since diurnal variability is a relatively insignificant factor in the oceans, e.g. Warsh et al. (1971) and Pollard (1980). Their diminution, following a storm or frontal passage, is most likely a combination of at least three factors: frictional dissipation, horizontal energy dispersion, in which the amplitude decays like t^{-1} (Whitham, 1974, Chapter 11) and vertical energy dispersion to underlying stratified layers where the energy is carried away by internal wave motions (Bell, 1978). The decay rates calculated for the latter process by Bell are about double the decay rates associated with the presence of the Ekman layer. Related work on vertical energy dispersion from frontal regions has also been reported by Wang (1991) and by Klein and Treguier (1993), although their models differ from the present one. Nevertheless, the fact that there are competing physical processes proposed to explain energy loss from oceanic oscillations presents a challenging analysis problem.

Acknowledgements

Financial support, provided in part by the National Science Foundation, Division of Atmospheric Sciences, Mesoscale Dynamics Program, is gratefully acknowledged. We also express our appreciation to John Hart for helpful comments offered during the course of this investigation, to Vern Ostdiek for supplying Fig. 2, and to an anonymous reviewer for several comments that have improved the clarity of the presentation.

Appendix A. Ekman suction velocity

The vertical velocity at the top of the Ekman layer, found by integration of the continuity equation, is

$$w_{\rm B} = -\int_0^{D_{\rm E}} \frac{\partial u}{\partial x} \, \mathrm{d}z,\tag{A.1}$$

where w=0 at z=0 and $D_{\rm E}\approx\pi\,\delta_{\rm E}$ is essentially the depth of the Ekman layer. The boundary layer solution (19) consists of two contributions. The first two expressions provide the Ekman boundary layer response, consisting of cross-isobaric flow. The second contribution, contained in the third expression, provides the expression at the top of the boundary layer (18), which matches the inviscid solution (17) in the upper layer. Neither the geostrophic flow nor the inertial oscillation provide Ekman layer convergence, which contributes to a finite $w_{\rm B}$ in Eq. (A.1). The ageostrophic departure from this latter contribution is used to evaluate Eq. (A.1).

The contributions from these integrals are aided by the use of the complementary error function $\operatorname{erfc}(y) = 1 - \operatorname{erf}(y)$, where $\operatorname{erfc}(y)$ is defined by (20). Then the contribution from the first integral is

$$I_{1} = \frac{1}{2} (1 - i) [e^{(1+i)D_{E}/\delta_{E}} - 1]$$

$$- \int_{(1+i)ft}^{D_{E}/\delta_{E} + (1+i)ft} \exp[-2ift + (1+i)\eta] \operatorname{erf} \left[\frac{\eta}{2} \left(\frac{ft}{2} \right)^{-1} \right] d\eta, \tag{A.2}$$

where $\eta = z/\delta_E + (1+i)ft$. The integral in (A.2) is provided in Gautschi (1964, 7.4.36). Evaluation at the two limits yields

$$I_{1} = \frac{1}{2} (1 - i) \left[e^{(1+i)D_{E}/\delta_{E}} - 1 \right]$$

$$-\frac{1}{2} (1 - i) \left\{ e^{(1+i)D_{E}/\delta_{E}} \operatorname{erf} \left[\frac{1}{2} \left(\frac{ft}{2} \right)^{-1/2} \left(\frac{D_{E}}{\delta_{E}} + (1+i)ft \right) \right] - e^{-ift} \operatorname{erf} \left[\frac{D_{E}}{2\delta_{E}} \left(\frac{ft}{2} \right)^{-1/2} \right] - \operatorname{erf} \left[(1+i) \left(\frac{ft}{2} \right)^{1/2} \right] \right\}.$$
(A.3)

The second integral, found from (A.1) and (19), is evaluated similarly and is given by

$$I_{2} = -\frac{1}{2}(1-i)\left[e^{-(1+i)D_{E}/\delta_{E}} - 1\right] + \frac{1}{2}(1-i)\left\{e^{-(1+i)D_{E}/\delta_{E}}\operatorname{erf}\left[\frac{1}{2}\left(\frac{ft}{2}\right)^{-1/2}\left(\frac{D_{E}}{\delta_{E}} - (1+i)ft\right)\right] - e^{-ift}\operatorname{erf}\left[\frac{D_{E}}{2\delta_{E}}\left(\frac{ft}{2}\right)^{-1/2}\right] - \operatorname{erf}\left[-(1+i)\left(\frac{ft}{2}\right)^{1/2}\right]\right\}.$$
(A.4)

Consider ft finite and $D_{\rm E}/\delta_{\rm E} \to \infty$. The asymptotic expression (Gautschi, 1964; 7.1.23) is introduced into (A.3) and (A.4) with the result that (A.1) reduces to

$$w_{\rm B} \approx \Re \frac{\delta_{\rm E}}{2} \frac{\partial v_{\rm g}}{\partial x} (1+i) \operatorname{erf} \left[(1+i) \left(\frac{ft}{2} \right)^{1/2} \right].$$
 (A.5)

Finally, the error function in (A.5) is evaluated by means of Gautschi (1964, 7.1.29) to give (22).

References

- Andrews, D.G., Hoskins, B.J., 1978. Energy spectra predicted by semi-geostrophic theories of frontogenesis. J. Atmos. Sci. 35, 509–512.
- Banta, R.M., Senff, C.J., White, A.B., Trainer, M., McNider, R.T., Valente, R.J., Mayor, S.D., Alvarez, R.J., Hardesty, R.M., Parrish, D., Fehsenfeld, F.C., 1998. Daytime buildup and nighttime transport of urban ozone in the boundary layer during a stagnation episode. J. Geophys. Res. 103, 22519–22544.
- Blackadar, A.K., 1957. Boundary layer wind maxima and their significance for the growth of nocturnal inversions. Bull. Am. Meteorol. Soc. 38, 283–290.
- Bell, T.H., 1978. Radiation damping of inertial oscillations in the upper ocean. J. Fluid Mech. 88, 289-308.
- Blumen, W., 1997. A model of inertial oscillations with deformation frontogenesis. J. Atmos. Sci. 54, 2681–2692.
- Blumen, W., 2000. Inertial oscillations and frontogenesis in a zero potential vorticity model. J. Phys. Oceanogr. 30, 31–39.
- Blumen, W., Gamage, N., Grossman, R.L., LeMone, M.A., Miller, L.J., 1996. The low-level structure and evolution of a dry arctic front over the central United States. Part II. Comparison with theory. Monthly Wea. Rev. 124, 1676–1692.
- Cushman-Roisin, B., 1994. Introduction to Geophysical Fluid Dynamics. Prentice-Hall, Englewood Cliffs, NJ, 320 pp.
- Gautschi, W., 1964. The error function and Fresnel integrals. Handbook of Mathematical Functions. National Bureau of Standards, Applied Mathematics Series, No. 55. US Government Printing Office, Washington, DC, pp. 295–319.
- Greenspan, H.P., 1990. The Theory of Rotating Fluids. Breukelen Press, Brookline, 325 pp.
- Hart, J.E., 2000. A note on nonlinear corrections to the Ekman layer pumping velocity. Phys. Fluids 12, 131-135.
- Holton, J.R., 1992. An Introduction to Dynamic Meteorology, 3rd Edition. Academic Press, San Diego, 507 pp.
- Hoskins, B.J., 1975. The geostrophic momentum approximation and the semigeostrophic equations. J. Atmos. Sci. 32, 233–242.
- Hoskins, B.J., Draghici, I., 1977. The forcing of ageostrophic motion according to the semi-geostrophic equations in an isentropic coordinate model. J. Atmos. Sci. 34, 1859–1867.
- Klein, P., Treguier, A.M., 1993. Inertial resonance induced by an oceanic front. J. Phys. Oceanogr. 23, 1897–1915.
- Kundu, P.K., Thomson, R.E., 1985. Inertial oscillations due to a moving front. J. Phys. Oceanogr. 15, 1076-1084.
- Kunze, E., Sanford, T.B., 1984. Observations of near inertial waves in a front. J. Phys. Oceanogr. 14, 566-581.
- Lighthill, J., 1978. Waves in Fluids. University Press, Cambridge, 504 pp.
- Mori, Y., 1990. Evidence of inertial oscillations of the surface wind at Marcus Island. J. Geophys. Res. 95 (11), 777–783.
- Ostdiek, V., Blumen, W., 1997. A dynamic trio:inertial oscillation, deformation frontogenesis, and the Ekman–Taylor boundary layer. J. Atmos. Sci. 54, 1490–1502.
- Pandolfo, J.P., Brown, P.S., 1967. Inertial oscillations in an Ekman layer containing a horizontal discontinuity surface. J. Mar. Res. 25, 10–28.
- Pedlosky, J., 1987. Geophysical Fluid Dynamics, 2nd Edition. Springer, New York, 710 pp.
- Pollard, R.T., 1980. Properties of near-surface inertial oscillations. J. Phys. Oceanogr. 10, 385–398.
- Sanders, F., 1999. A short-lived cold front in the Southwestern United States. Monthly Wea. Rev. 127, 2395–2403.
- Singh, M.P., McNider, R.T., Lin, J.T., 1993. An analytical study of diurnal wind-structure variations in the boundary layer and the low-level jet. Bound-Layer Meteorol. 63, 397–423.
- Tandon, A., Garrett, C., 1994. Mixed layer restratification due to a horizontal temperature gradient. J. Phys. Oceanogr. 24, 1419–1424.
- Thorpe, A.J., Guymer, T.H., 1977. The nocturnal jet. Q. J. R. Meteorol. Soc. 103, 633-653.
- Wang, D.-P., 1991. Generation and propagation in a subtropical front. J. Mar. Res. 49, 619–633.
- Warsh, K.L., Echternacht, K.L., Garstang, M., 1971. Structure of near surface currents east of Barbados. J. Phys. Oceanogr. 1, 123–129.
- Whitham, G.B., 1974. Linear and Nonlinear Waves. Wiley, New York, 636 pp.